Period Times and Helix Alignment during the Cyclic Migration of DNA in Electrophoresis Gels Studied with Fluorescence Microscopy

Anette Larsson and Björn Åkerman*

Department of Physical Chemistry, Chalmers University of Technology, S-41296 Göteborg, Sweden

Received December 12, 1994; Revised Manuscript Received April 5, 1995[⊗]

ABSTRACT: Fluorescence microscopy of YOYO-stained DNA molecules has been used to study the periodicity of the cyclic migration during constant field electrophoresis in agarose gels. The distribution of period times is asymmetric and wide, with a ratio of standard deviation to mean value of 0.50 for fields between 3 and 24 V/cm. The average period time decreases with the electric field strength, E, as $E^{-1.2}$, and increases with increasing molecular weight (38−740 kbp) and increasing gel concentration (0.5−2%). The period times for T2 DNA (164 kbp) are in good agreement with the time to the orientation undershoot, as measured in a separate linear dichroism study of YOYO-stained DNA undergoing ordinary zone electrophoresis (Carlsson et al., manuscript in preparation). This shows that linear dichroism can be used to quantify the period time of the cyclic motion and to investigate effects of changes in DNA or gel properties. The cyclic conformational changes in the global DNA conformation during migration have been characterized in terms of the apparent length L_μ and end-to-end distance h_μ of the molecular paths in the gel. The formation of U conformations dominates the cycle time, since it is slow compared to U slipping and retraction. The maximum and cycle-averaged orientation factors for the apparent molecular path are evaluated from the images to be 0.70 and 0.67 ± 0.03, respectively, for T2 DNA at 8 V/cm in 1% agarose. From these values the degree of helix orientation below the level of microscope resolution could be estimated by comparison with the total orientation factor for the DNA helix as measured with linear dichroism. The maximum and cycle-averaged orientation factor for the helix with respect to the global path were 0.27 and 0.22 ± 0.01, respectively. These orientation factor values demonstrate (1) a very high degree of field alignment of the global path and (2) a degree of stretching of the helix along that path which is considerable, and stronger than expected for a wormlike chain spanning a cavity with the average pore size. If the imaged path corresponds to the reptation tube, the estimated friction coefficient for motion along the tube is found to be close to the value in the buffer.

Introduction

Gel electrophoresis of DNA has become an intensive area of research[1−3] since the discovery that pulsing the electric field dramatically improves the separation of Mbp DNA molecules.[4,5] Polarized spectroscopy, such as linear dichroism (LD), has shown that long DNA molecules become highly oriented by the migration through the gel,[6,7] and spectroscopic studies,[8−11] together with simulations,[12−16] have shown that reorientation between the alternating field directions is involved in the mechanism responsible for the improved separation in pulsed field electrophoresis. More recently, fluorescence microscopy observation of individual molecules has been employed, e.g. to verify[17] the separation mechanism suggested for field inversion electrophoresis on the basis of spectroscopy[8] and simulations.[12,14,18,19]

A more fundamental discovery with microscopy was that even in a constant field long DNA molecules migrate in an oscillatory manner,[20,21] confirming predictions from computer simulations of linear polymers moving in a regular lattice.[13] This kind of extension−contraction motion, termed geometration,[18] explained the oscillations in the DNA orientation that were observed spectroscopically at the beginning of a field pulse.[7,22] The oscillatory alignment of the DNA helix can be followed by a macroscopic technique only if the ensemble performs the cyclic conversions in concert to a certain degree,[15,18,22] which happens only initially in a field pulse when applied to equilibrated molecules that can respond in a coherent fashion.[23] During continued migration the coherence between the molecules is lost due to the stochastic nature of the interaction with the gel network and only the cycle-averaged orientation is observed as a consequence of the ensemble-averaging, although each molecule continues to oscillate. In this study we determine the distribution of period times for the geometration by microscopy and compare them with the oscillation observed by LD.

Once the ambiguities due to the averaging have been removed, spectroscopic methods are powerful for mechanistic studies, as exemplified by an extensive classification of migration modes of DNA between 6 and 164 kbp based on LD dynamics,[24] which would not be feasible using microscopy. A more fundamental limitation in microscopy is the resolution. Spectroscopic and mobility studies indicate[1] that important modes of motion of the DNA chains occur on length and time scales below the spatial (2500 Å[25,26]) and temporal (25 images/s) resolution in the video images. Being a spectroscopic technique, LD does not involve imaging and, hence, helix alignment is detected on all length scales (and with a temporal resolution of typically 1 ms). As a consequence, LD reflects both the *global* alignment of the molecular path in the gel and the degree of *local* helix orientation of the DNA in the pores. In this study we extract information about the DNA conformation at the pore level from LD, by using microscopy data on the global orientation. An interesting aspect of this approach is that the division between global and local conformation based on microscope resolution closely mimics the division between tube and intratube DNA

* To whom correspondence should be addressed.
[⊗] Abstract published in *Advance ACS Abstracts,* May 15, 1995.

0024-9297/95/2228-4441$09.00/0

conformation in reptation theories.

Spectroscopy and microscopy are of complementary nature: microscopy gives mechanistic insight at the molecular level about the distribution of global conformation, whereas spectroscopy efficiently provides statistically significant data on the average DNA behavior. The power of their combination has only started to provide insight into molecular mechanisms underlying migration and separation of DNA in gels, and so far usually by collection of data from separate studies. An important exception is the work by Holzwarth and coworkers[27,28] on the electrophoretic velocity. In this study we concentrate on the electrophoretic orientation of the DNA molecules by combining microscopy and spectroscopy data obtained on the same system.

Experimental Section

Chemicals and Sample Preparation. G bacteriophage DNA (740 kbp)[29] was kindly prepared by Chantal Turmel, Xerox Co, Montreal, as described previously;[22] DNA of T2 (164 kbp) and T7 (38 kbp) bacteriophages were purchased from Sigma, and YOYO-1 was obtained from Molecular Probes, Eugene, OR. All samples were used as received. Agarose of Ultra DNA grade from Biorad and 50 mM TBE buffer (50 mM Tris, 50 mM boric acid, and 1.25 mM EDTA) were used in all experiments. From an argon-bubbled (1 min) sample of 980 μL of 1% agarose (50 °C), 20 μL of β-mercaptoethanol, and 2 μL of YOYO–DNA solution (0.6 μM YOYO and 6.0 μM DNA bases), 20 μL was used to form a 40 μm thick gel on a heated (*ca.* 60 °C) and argon-fluxed microscope slide by applying a 22 × 22 mm^2 cover slip. Two of the edges were sealed with fingernail polish, and two platinum wire electrodes (28 mm apart), perpendicular to the sealed edges and electrically connected to the sample gel by use of agarose gel, were fed from a voltage-stabilized power supply. The slide package was kept for 15 min at 20 °C before observations started. In field inversion electrophoresis (1% agarose slab gel, 7.5 V/cm, T_+: T_- = 3 s:1.5 s), the T7 and G-phage samples migrated as one band, whereas the T2 sample contained a major (intact T2) and a minor component (approximately 70–90 kbp in size).

Fluorescence Microscopy. Images obtained in a Zeiss Axioplan microscope (100× Plan-Neofluar, NA = 1.3, and 2× Optovar lens) by excitation at 450–490 nm and emission above 520 nm, were recorded using an image-intensified video camera (GenIISys VE-1000 system, DAGE-MTI Inc.), time coded (time resolution 0.04 s) by an Argus 10 image processor (Hamamatsu) and stored on video tape (Panasonic, AG-7330). Only molecules in the middle of the microgel were studied, since in the central part of such a sample the migration is very similar to that in bulk gels.[28,30]

Distributions of the period time for the cyclic motion, determined by measuring consecutive time lapses between compact conformations as described in more detail in the Results, were based on typically 50–300 observations of on average 10 different molecules, at each field strength. The length L_μ and end-to-end distance h_μ of the apparent path of the DNA molecules in the images (called the μpath) were measured using a tracing option in the image processor, calibrated by a microscope ruler (Graticules LTD), in 60 randomly chosen images during 1 min of a representative DNA migration sequence at 8 V/cm. The three-dimensional μpath is longer than the projected length measured in the image plane, but corrections are less than 5% under present conditions (Appendix). The μpath data are limited to observations on one molecule (going through many cycles), which had an average period time (6.9 s) close to the average observed over many molecules (6.3 s). Furthermore, the maximum μpath lengths we observe are incompatible with a contour length corresponding to 90 kbp, so the studied molecule belongs to the major component of intact T2 molecules. Segmental orientation of the μpath with respect to the field direction at 3 V/cm was determined by dividing the molecule image into straight segments of equal apparent lengths (1.5 μm).

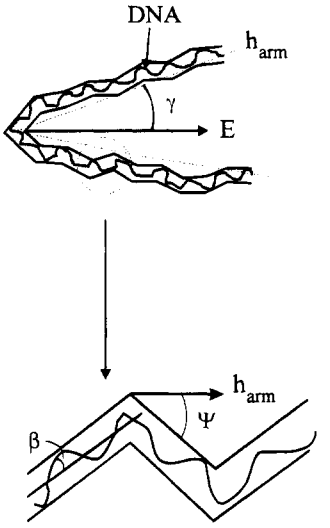

Figure 1. Definition of angles γ, ψ, and β (in three dimensions) for the orientation parameters S_{apex}, S_μ, and S_{local}, respectively. The angles γ' and ψ', used in eq 4, denote the corresponding angles in the image plane.

Linear Dichroism Theory

Linear dichroism (LD), the difference in absorption of light plane-polarized parallel and perpendicular to the field direction, respectively, is a measure of the orientation of the helix axis with respect to the field. The reduced linear dichroism LD^r (LD divided by the absorbance in absence of field[31]) of a certain DNA conformation is given by the product of an orientation factor, S, describing the orientation of the helix axis with respect to the field, and an optical factor, O, that describes the orientation of the transition moments (for the transition responsible for the absorption at the wavelength used) with respect to the local helix axis:[31]

$$LD^r = O \times S = 3\frac{(3\langle\cos^2\alpha\rangle - 1)}{2} \times \frac{(3\langle\cos^2\theta\rangle - 1)}{2} \quad (1)$$

The angle α, between the transition moment and the helix axis, is averaged over all transitions, whereas θ, the angle between the DNA helix axis and the electric field direction, is averaged along the chain in the actual conformation and over the ensemble for a collection of molecules. S varies between 0, for random orientation, and 1, for perfect field alignment of the helix axis. Electrophoretic alignment of DNA is never perfect,[1] and Figure 1 illustrates how can this can be attributed to the lack of perfect orientation on three different levels (characterized by the angles β, ψ, and γ). Due to resolution limitations[25] the DNA conformation is imaged as a coarse-grained representation (the μpath), which will be referred to as the global DNA conformation. Instead of using S, that directly relates the helix orientation to the field, we will therefore consider separately the *local orientation*, i.e. alignment of the helix with respect to the local axis of the μpath (β), and the *global orientation*, i.e. the alignment of the μpath axis with respect to the field direction. The total orientation factor for the DNA helix, S, then factorizes into local and global orientation contributions[31] (under assumptions to be discussed in section C2 of the discussion)

$$S = S_{global}S_{local} \quad (2)$$

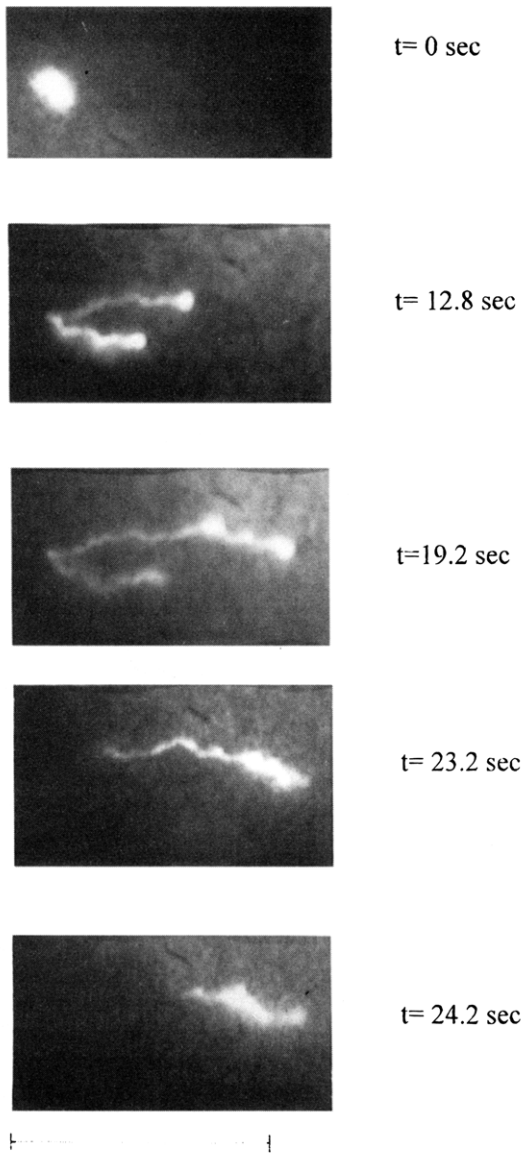

Figure 2. Images of a YOYO-stained T2 DNA molecule (contour length 78.1 μm) at 3 V/cm in 1% agarose gel. The bar is 30 μm, and the elapsed time is indicated. Top to bottom: (a) A compact conformation. (b) The DNA molecule is hooked around a gel fiber and becomes elongated by the electric field forces. (c) The two arms are involved in a tug-of-war, and the upper arm wins. (d) The upper arm has pulled the lower arm around the gel fiber, and the molecule contracts. (e) A new compact conformation.

Sometimes in the microscopy images the μpath is observed to consist of two arms in a distinct V-shaped conformation (Figure 2). As will be seen below, under present circumstances this represents a small deviation from perfect orientation, but it has to be taken into account in a complete treatment of the LD. The orientation of the μpath with respect to the field direction (S_{global}) therefore in turn has two contributions, giving rise to two orientation factors: the orientation of the end-to-end vector of the arm with respect to the field (angle γ, orientation factor S_{apex}) and the orientation of the μpath with respect to the end-to-end vector of the arm (angle ψ, orientation factor S_μ). The total orientation factor in eq 1 then is given by the product[31]

$$S = S_{apex} S_\mu S_{local} \qquad (3)$$

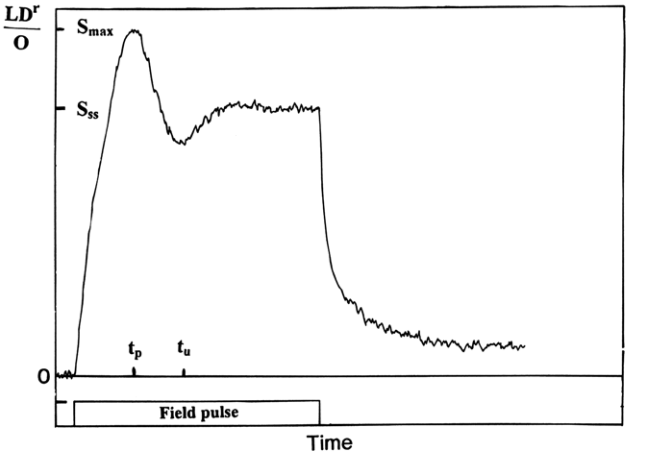

Figure 3. Typical LD response of T2 DNA (starting as equilibrium coils) to a constant field pulse.[22] S_{max} and S_{ss} are the maximum and steady state value of LD^r/O, respectively. t_p and t_u are the times (starting from field application) to reach the maximum and minimum LD, respectively.

The orientation factors S_μ, S_{apex}, and S_{local} depend on the three-dimensional angles ψ, γ, and β, respectively, through the same type of expression as given for S in eq 1. However, microscopy can only provide values for the corresponding two-dimensional angles ψ' and γ'. The orientation factors S_{apex} and S_μ need therefore to be expressed in ψ' and γ' (Appendix), while the orientation factor S_{local} is expressed in the three-dimensional angle β (which cannot be measured due to resolution limitations):

$$S_{apex} = (2\langle\cos^2(\gamma')\rangle - 1)/(2 - \langle\cos^2(\gamma')\rangle) \qquad (4a)$$

$$S_\mu = (2\langle\cos^2(\psi')\rangle - 1)/(2 - \langle\cos^2(\psi')\rangle) \qquad (4b)$$

$$S_{local} = (3\langle\cos^2(\beta)\rangle - 1)/2 \qquad (4c)$$

For T2 DNA stained with YOYO to the same extent as in the present microscopy studies, the LD response for DNA starting from equilibrium (obtained, as described elsewhere,[22] by Carlsson et al.[32]) exhibits the same kind of oscillatory behavior as native DNA[22] (Figure 3, where the maximum (S_{max}) and steady state (S_{ss}) orientation factors are defined). Since YOYO is bisintercalated, the transition moments of both chromophores are essentially perpendicular to the helix axis ($\alpha = 90°$),[33,34] and LD^r values measured at 490 nm, where only YOYO and not DNA absorbs, are therefore converted into orientation factors by using a value of -1.5 for the optical factor in eq 1, to be approximately $S_{max} = 0.19$ and $S_{ss} = 0.15$ for YOYO-stained T2 DNA at 8 V/cm in 1% agarose gel.[35]

Results

A. DNA Conformations during the Cycle. Representative images of the commonly observed[20,21,28,36–39] oscillations between compressed and extended conformations during a migration cycle are presented for T2 DNA in Figure 2. Figure 2a shows a compressed conformation, whereas in Figure 2b,c the molecule first becomes hooked around a gel fiber (U conformation) and then slips around the pivot point (J conformation), pulled by the longest arm. Finally, the shorter arm slips off the gel fiber, and the DNA molecule contracts into a new compressed conformation (Figure 2d,e). Sometimes, the arms of a hooked conformation are off-field

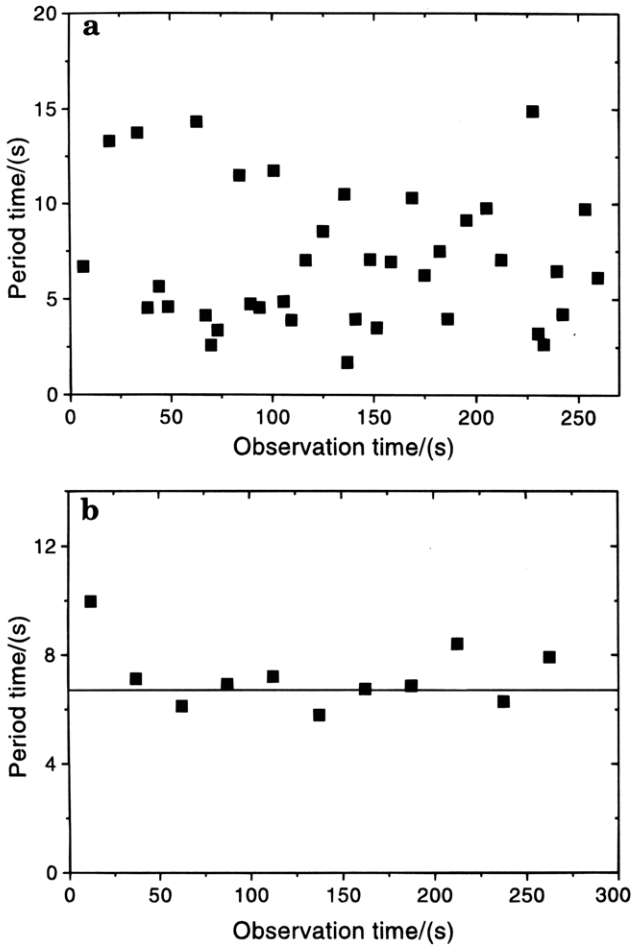

Figure 4. (a) Period time for a YOYO–T2 DNA molecule at 8 V/cm in 1% agarose determined for consecutive cycles and plotted versus the observation time. (b) Period time data from (a), averaged in intervals of 25 s, versus the observation time. The line corresponds to the total average at 8 V/cm.

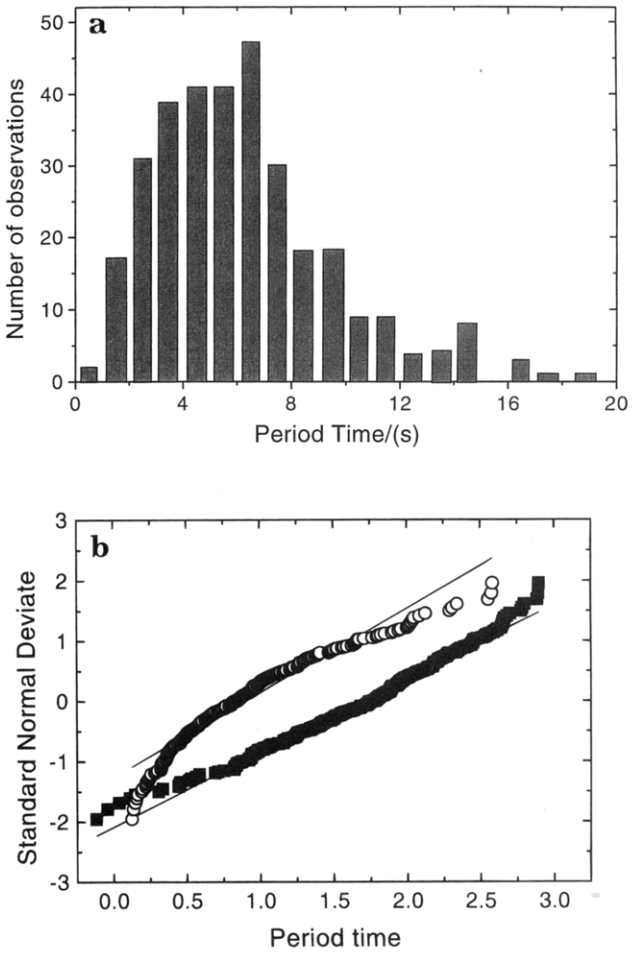

Figure 5. Histogram of the period time for YOYO–T2 DNA at 8 V/cm in 1% agarose. Each bin corresponds to 1 s. Total of 351 observations on 10 different molecules. (b) Normal probability plot of the period times (○) and the natural logarithm of the period times (■). (The lines are least-squares fits to the experimental data.) In this presentation a straight line indicates that the stochastic variable follows a normal distribution,[40] which is seen to be a better description of the natural logarithm of the period time than of the period time.

in opposite directions, in a V-type global shape also observed by Rampino.[38] We also note (Figure 2c,d) that the leading end is bright when the molecule slips and contracts (as is commonly observed[20,21,28,36]) but that the leading parts in *both* arms are bright as the U forms are generated (Figure 2b). T7 DNA oscillates in a similar manner, but faster. In contrast, G-DNA often exhibits branched conformations with several heads, although the migration is still clearly cyclic.

The coarse-grained representation of the DNA conformation as represented by the μpath in Figure 2 was used to evaluate the period times of the cycle, and the degree of global field alignment of the DNA.

B. Period Time. B1. Distribution of the Period Times. We define the time between two compressed conformations in a migration cycle as the period time, since comparison will be made with LD responses starting from coiled conformations. Compressed conformations are well-defined except in the few (<5% for T2 and T7, more for G-DNA) cases when the migration cycle included a branched Y conformation, which occurs if a new entanglement point starts to develop before the trailing part has slipped off the old. Since the hooking point in the tail is normally released first and the molecule evolves into an ordinary U conformation, we have chosen to regard these Y conformations as defining the start of a new cycle.

A sequence of measured period times at 8 V/cm is plotted versus observation time in Figure 4a, where the scatter shows that the period time distribution is wide. The short-time (25 s) averaged period time does not change systematically during the observation time (260 s) (Figure 4b), which indicates that the electric field is stable and that no damage has occurred to the DNA molecule. The autocorrelation function for the duration of consequtive cycles was calculated as[40]

$$a_{\mathrm{corr}} = \frac{\sum(t_i - \bar{t})(t_{i+1} - \bar{t})}{\sum(t_i - \bar{t})^2} \tag{5}$$

where t_i and t_{i+1} are consecutive period times. We obtain $a_{\mathrm{corr}} = -0.12$, for a set of 254 observations in sequences extending over at least 30 cycles, which corresponds to a 97.5% confidence interval of ± 0.12. A value of a_{corr} outside this interval means that the period times are correlated, and thus we cannot exclude, at the 97.5% confidence level, the possibility that the period times are correlated, but if such a correlation exists it is low and negative.

The distribution of period times at 8 V/cm (Figure 5a) is wide and asymmetric (mean and median times of 6.3 and 5.9 s, respectively, and standard deviation 3.4 s) and is in fact quite well described by a log-normal distribution (Figure 5b). In terms of molecular confor-

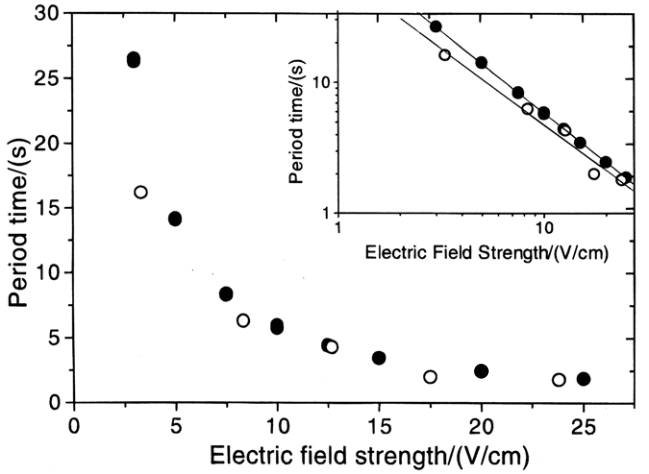

Figure 6. Dependence of the period time on the electric field strength for YOYO–T2 DNA in 1% agarose determined by microscopy (○, this work) and by LD (●, ref 32). DNA concentrations were 6 nM bases in microscopy and less than 0.10 mM bases in LD. The numbers of observations in the microscopy experiments were 87 (3 V/cm), 351 (8 V/cm), 123 (13 V/cm), 89 (18 V/cm), and 30 (24 V/cm). The inset shows that the LD data and the microscopy data decrease with the electric field strength as $E^{-1.26}$ and $E^{-1.16}$, respectively.

Table 1. Average Period Times[a]

DNA size[b]	av period time (s)
38	1.9 ± 0.8
164	6.3 ± 3.4
740	13.0 ± 7.8
gel conc[c] (%)	**av period time (s)**
0.7	4.0 ± 2.1
1.0	6.3 ± 3.4
1.5	7.6 ± 4.0

[a] YOYO-stained DNA (phosphate–dye ratio 10), 8 V/cm. [b] 1% agarose. [c] DNA size 164 kbp.

mations, the lowest 5% of the period times arose from a migration cycle involving a Y conformation, whereas the longest period times correspond to molecules hooked with approximately two equal arms. The period-time distribution shifted consistently to shorter times as the field was increased between 3 and 24 V/cm. The asymmetric and wide shape was retained, however, with a ratio between standard deviation and mean values equal to 0.50 ± 0.02 in this field range.

B2. Average Period Time. Figure 6 shows that the average period time for T2 DNA molecules in 1% agarose gel decreases (as approximately $E^{-1.2}$) with increasing electric field strength, as an elevated electric field pulls the DNA through the conformational changes more rapidly. Longer DNA molecules have longer average periods (Table 1), since the molecules have to be pulled a further distance to complete a cycle, and Table 1 also shows how the period time becomes longer as the gel concentration is increased. Finally, from Table 1 it is clear that the period-time distribution is wide, with a ratio between standard deviation and the mean of about 0.5, in a wide range of DNA sizes and gel concentrations.

C. Molecular Alignment. C1. Distribution of the Contour Length and End-to-End Distance of the μpath. The distribution of the apparent contour length L_μ of the μpath for a T2 DNA molecule migrating at 8 V/cm (Figure 7a) is approximately symmetric. The average μpath length is 29.9 μm, and the maximum value 55 μm. This is 40 and 80%, respectively, of the

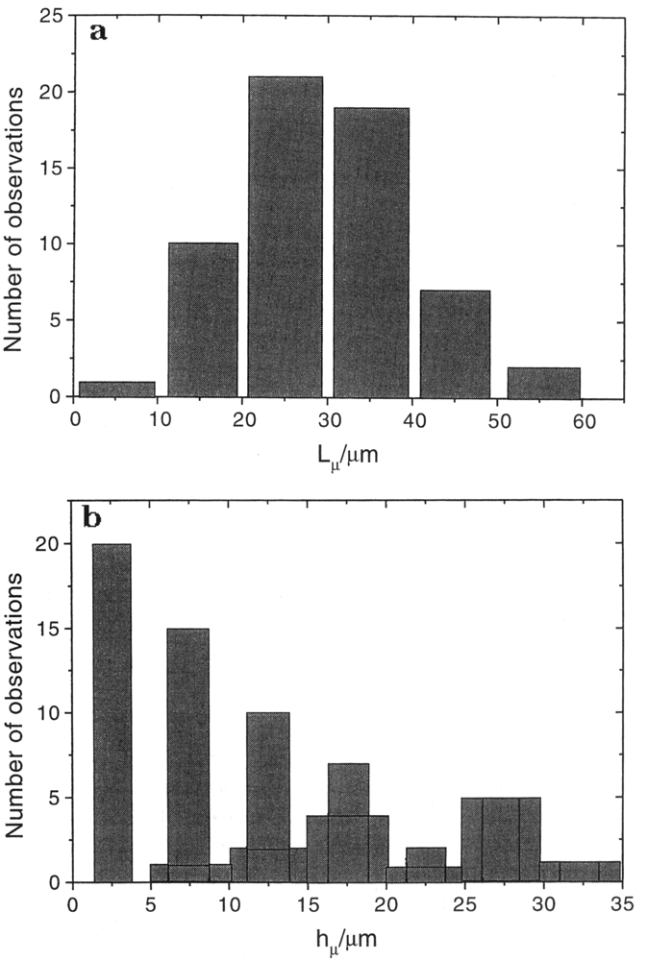

Figure 7. The length, L_μ, and the end-to-end distance, h_μ, of the μpath measured on 60 randomly chosen images from a 1-min sequence (approximately 10 cycles) of a YOYO–T2 DNA molecule, migrating at 8 V/cm in 1% agarose gel. (a) Histogram of L_μ, bin size 10 μm. (b) Histogram of h_μ, bin size 5 μm. Narrow bins correspond to all 60 conformations, whereas the wide bins correspond to the 13 I conformations.

Table 2. Cycle-Averaged μpath Parameters[a]

$\langle L_\mu \rangle$ (μm)	(29.9 ± 10.7)
$\sqrt{\langle h_\mu^2 \rangle}$ (μm)	(13.4 ± 15.8)
$\langle h_\mu / L_\mu \rangle$	0.40 ± 0.32
$\langle h_\mu^2 / L_\mu^2 \rangle$	0.25 ± 0.34
$\langle h_\mu^2 / L_c L_\mu \rangle$	0.082 ± 0.110

[a] YOYO-stained T2 DNA (phosphate–dye ratio 10) at 8 V/cm in 1% agarose.

contour length of the YOYO-stained T2 DNA, which is 78.1 μm when a 22.3 μm extension (3.4 Å/chromophore[41]) is included for the present degree of staining with the bisintercalated YOYO.[33] These values demonstrate quantitatively the large degree of extension of the DNA coils during electrophoretic migration at field strengths typically used for separation, which is also evident from comparing the average value of 13.4 μm for the end-to-end distance of the μpath ($\langle h_\mu^2 \rangle$) to the calculated equilibrium value of 2.8 μm for YOYO-stained T2 DNA (wormlike-chain model without excluded volume,[42] 500 Å persistence length[43]). The distribution of h_μ (Figure 7b) is clearly asymmetric (the median value (8.5 μm) is 30% smaller than the average value), because both compact and nearly symmetric U conformations have small values of h_μ. The cycle-averaged values of some relevant μpath parameters are summarized in Table 2, where the large standard deviations reflect the strong fluctuations in the μpath properties over the cycle.

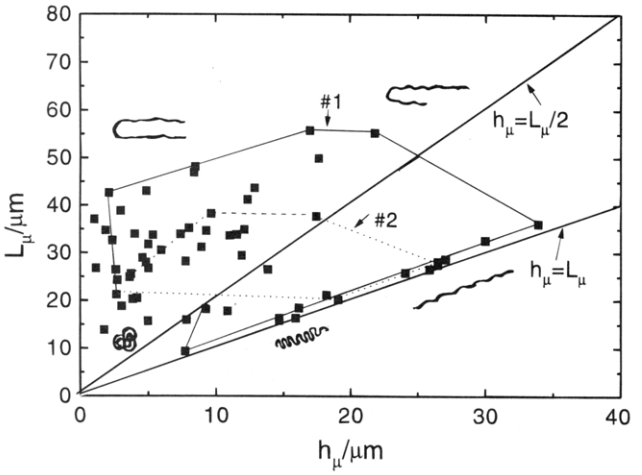

Figure 8. Length of the μpath, L_μ, plotted versus the end-to-end distance, h_μ, for each conformation. The curves connect points corresponding to two complete migration cycles. Path 1 (solid) corresponds to a cycle including a nearly symmetric U, whereas path 2 (dashed) represents a cycle involving a less symmetric U conformation. Experimental conditions are as in Figure 7.

C2. Migration Cycle in the h_μ–L_μ Conformational Space. The time evolution of the μpath conformation is well illustrated by plotting L_μ versus h_μ. This is done for 60 conformations (observed at 8 V/cm) in Figure 8, which approximately represents the distribution of conformations (characterized in terms of h_μ and L_μ) over the migration cycle, since the images were sampled randomly, and over an interval that is much longer than the average cycle time. The typical conformations from Figure 2 (depicted in cartoon form in Figure 8) split into two groups. One group is spread out along the line $h_\mu = L_\mu$ and corresponds to I-shaped molecules in different states of contraction. The other group is more widely spread mainly in the area $h_\mu < L_\mu/2$. These conformations are either symmetric with small h_μ (U) or have progressively higher degrees of arm asymmetry as h_μ increases (J), with the L_μ value giving a rough estimate of the degree of stretching in the arms. In particular, the compact states are observed at L_μ = 5–15 μm, where the two groups meet.

When the points are connected (1 per s on the average, or six samplings per average cycle), the migration cycle can be identified as a set of closed paths corresponding to an evolution through the typical cycle states: coil–U–J–I–coil. If this sequence is followed faithfully, the path forms a wide arc (no. 1 in Figure 8), whereas it becomes narrower and/or distorted (no. 2 in Figure 8) if the U is asymmetric from the start or if Y conformations are involved.

C3. Segmental Orientation. Figure 9a gives the distribution of the angle ψ' between the μpath segments and the end-to-end vector of five different arms of two U conformations and one I conformation. In the three conformations investigated, the angle γ' between the end-to-end vector of the five arms and the field direction varied between 4.8 and 8.3°, with an average of 6.5°, corresponding to an apex angle of $2\gamma' = 13°$. We have not made a systematic study of the apex angle, but visual inspection of a large set of images shows that a majority of the conformations have apex angles smaller than the average value 13° obtained here. A value of $\gamma' = 6.5°$ gives $S_{apex} = 0.96$ according to eq 4a, so the deviation from 1 is smaller than the uncertainties in the determination of S_μ (see below). We will therefore neglect the effect of the apex angles on the LD and set $S_{apex} = 1$, which in effect amounts to redefining ψ' as the angle between the μpath axis and the field direction rather than the arm direction.

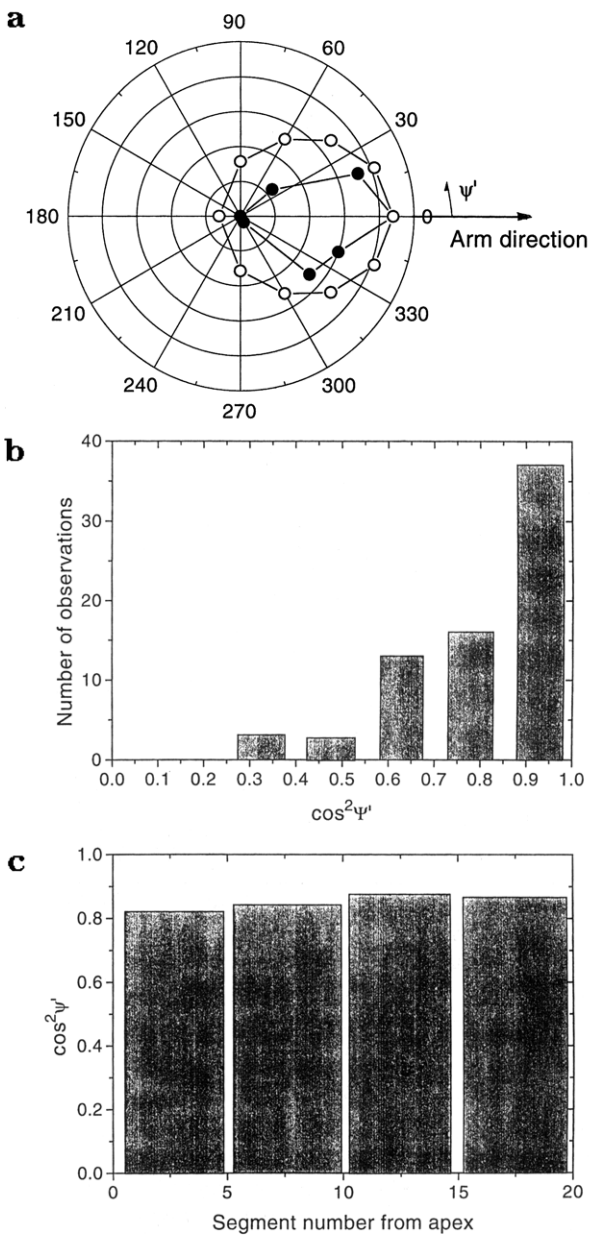

Figure 9. Distribution of the angle ψ' between the μpath segments (73 segments of 1.5 μm apparent length) and the end-to-end vector of the arms, in two U conformations and one I conformation at 3 V/cm in 1% agarose. (a) Polar representation of the ψ' distribution. Experimental data (bin = 20°) (●) and values (○) predicted by the Kuhn–Grün model at h/L = 0.3 (from Figure 7b in ref 58). (b) Distribution of $\cos^2\psi'$ (bin = 0.15). (c) Variation of $\cos^2\psi'$ over the length of the arms (bin = 5 segments).

Figure 9a shows that the distribution of ψ' is strongly biased, with all segments being within 60° of the field direction, and with an average value $\langle|\psi'|\rangle$ of 19.1°. Figure 9b shows the distribution of $\cos^2\psi'$, which governs the contribution to LD from μpath alignment according to (4b). Figure 9c shows that $\langle\cos^2\psi'\rangle$ varies by 10% along the length of the arms, but without any trend outside the experimental uncertainties. The data on segmental orientation are summarized in Table 3.

Table 3. Segmental Orientation in 5 Arms of Extended Conformations[a]

arm[b]	N[c]	$\langle\cos^2\psi'\rangle$[d]	$(h/L)^2$[e]	error[f]
1	18	0.85 ± 0.17	0.86	1.02
2	13	0.69 ± 0.16	0.67	0.97
3	21	0.83 ± 0.15	0.77	0.94
4	12	0.87 ± 0.14	0.88	1.02
5	9	0.83 ± 0.22	0.79	0.95
av[g]		0.81 ± 0.17	0.80 ± 0.08	0.98 ± 0.04

[a] YOYO-stained T2 DNA (phosphate–dye ratio 10) at 3 V/cm in 1% agarose. [b] Arms 1 and 2 and arms 4 and 5 constituted two U conformations; arm 3, an I conformation. [c] Number of μpath segments. [d] The angle ψ' is between the segment and the direction of the end-to-end vector of the arm (Figure 1). [e] Ratio of the end-to-end distance and contour length of arm. [f] Ratio $(h/L)^2/\langle\cos^2\psi'\rangle$. [g] Average over the 5 arms.

Discussion

A. Global and Local DNA Conformation. Relation between the μpath and the Reptation Tube. Even in the most extended conformations the length of the μpath (Figure 7a) is considerably shorter than the DNA contour length (78 μm) and, averaged over the cycle L_μ, is only about half this value. Thus, on the average about half of the DNA chain length is hidden in undulations at levels below the resolution limit. This is consistent with the radius of curvature of the DNA chain in equilibrium (equal to the persistence length) being only 500 Å,[43] and thus less than the resolution limit of the microscope. Furthermore, DNA segments on this length scale move too fast (in the millisecond range[44,45]) to be imaged at the video rate, resulting in the conformation being smeared out. The important conclusion is that the fraction of the DNA conformation that cannot be imaged directly is significant. The DNA behavior on short length (~2000 Å) and time scales (<0.1 s) is likely to play an important role in gel electrophoresis, as indicated by effects of short field pulses on electrophoretic orientation and velocity[10,45] and zone widths,[46] and by studies of field-free orientation relaxation.[24] It is therefore important to find methods to characterize the part of the DNA conformation that cannot be imaged, which herein will be defined as the local conformation.

Although the local conformation is here defined by experimental limitations, it still represents a relevant division between global and local DNA orientation, because the μpath is expected to reflect approximately the conformation of the conceptually important reptation tube.[2] The topological constraints of the gel that are modeled by the tube are clearly reflected by the μpath, as evidenced by a strongly restricted Brownian motion lateral to the μpath of DNA in gels compared to the intense coil dynamics seen in images of molecules in free solution.[26,47,48] The Brownian motion of the μpath of DNA is concentrated polymer solutions is restricted in a way similar to that in gels[49] and has indeed been shown to be well described by reptation theories.[50] The μpath is expected to be a good representation of the topological constraints on the DNA motion during gel electrophoresis also, since similar limitations on the lateral motion are observed in the presence of the field. However, the μpath cannot be strictly identified with the reptation tube in agarose gels because the distance between topologically important gel fibers may be smaller than the average pore size (typically 2000 Å in 1% aragose)[51] and thus may be below the resolution limit in the video images. Details of the tube conformation may be lost in the images.

Keeping this potential resolution limitation in mind, we will regard the μpath as reflecting the global conformation, i.e., those elements of the DNA conformation that are controlled by the constraints of the gel matrix. On the other hand, the local DNA conformation at the pore level (inside the reptation tube) is smeared out because of resolution limitations and has to be studied by indirect methods. We will first analyze the global aspects of the cyclic motion and then extract information about the local conformation at different stages of the cycle.

B. Cyclic Motion. B1. Cycle Phases. Figure 8 offers a rough representation of the time the molecules spend in the different parts of the cycle, and most prominent is the lack of observations of highly asymmetric U shapes. The time curve of the molecule shows that the $h_\mu = L_\mu$ branch indeed is reached from the U conformations, and therefore the apparent lack of observations above $h_\mu = L_\mu/2$ must be the result of too infrequent image sampling. The data of Song and Maestre[52] show that at 8 V/cm the last half of the short arm of T2 DNA in a J conformation typically slips in less than 0.5 s (Figure 3 in ref 52), smaller indeed than our average sampling rate of 1 per s. Since the two ends move in opposite directions, h_μ changes even more rapidly whereas L_μ decreases only very slowly.[52] The slipping of a U conformation therefore corresponds to a more or less horizontal jump in Figure 8, and the lack of observed conformations between $h_\mu = L_\mu/2$ and $h_\mu = L_\mu$ thus reflects a rapid completion of this phase compared to the rest of the cycle.

When the tail slips around the pivot point, the contraction phase is entered, (observed by Song and Maestre[52] as the onset of a decrease in L_μ) during which the conformational change is slower, as evidenced by an increase in the number of observations in the I stage of Figure 8. A strict relation $h_\mu = L_\mu$ would imply a straight μpath. It is seen that h_μ is only slightly smaller than L_μ essentially throughout the contraction process ($h_\mu/L_\mu = 0.94$ as an average over all I conformations), as expected if the molecule contracts within an almost straight tube. The exact nature of the resulting compact states is uncertain, since the molecule strongly overlaps itself, so that h_μ and L_μ cannot be measured accurately. These projection limitations give rise to an uncharted region during the switch from I retraction to U formation, corresponding approximately to h_μ and L_μ being less than 10 μm (Appendix), where the μpath conformation is not known. Since less than 10% of the observed conformations fall within this range, the compact state as defined here is comparatively short-lived.

In contrast to the rapid slipping of the hooked conformation, a large fraction of the cycle is spent in building up the U forms, as evidenced by the comparatively high fraction of conformations observed in the U-formation phase. Studies of the recoiling of T4 DNA molecules (164 kbp, same length as T2) in 1% agarose gels indicate similarly that at 10 V/cm 40–60% of the molecules are in U-shaped conformations at any instant.[27] An almost vertical time curve, reflecting the formation of a nearly symmetric U are observed occasionally (no. 1 in Figure 8), but since U forms may rapidly become asymmetric the paths in general go through the broad region $h_\mu < L_\mu/2$ (not shown).

For the purpose of this study it is sufficient to observe that (1) a large fraction of the cycle is dedicated to U formation, (2) the excess of U conformations compared to J conformations shows that the process of U forma-

tion is slower than the U destruction, (3) the contraction in the I phase occurs essentially within a nearly straight μpath with $\langle h_\mu/L_\mu\rangle_I = 0.94$, and (4) the molecules spend about 10% of the cycle time in compact states.

B2. Average Period Time and the LD Response Time. Figure 5a shows that the width of the period-time distribution (e.g. the full width at half-maximum) is close to the average period time. Thus, for a set of molecules starting from a compact state at the same time, some will begin their second cycle already when the average molecule is only halfway through its first cycle. By contrast, the few molecules in the tail of the distribution will go through a cycle which may be more than twice as long as the average cycle and hence start their second cycle much after the average molecule. Consecutive period times are essentially uncorrelated according to our analysis (*vide supra*) and thus the coherence between most of the molecules will be lost after approximately one average cycle. This explains why molecules starting as equilibrium coils have a constant-field LD response that reaches a steady state level already after little more than one oscillation (Figure 3) and allows the interpretation that the initial LD oscillations reflect the ongoing geometration.

To test this interpretation directly, we compare in Figure 6 the period time obtained by microscopy with the apparent period time in the LD oscillations. As LD data we will use the time to the LD undershoot (t_u in Figure 3), which should correspond to the full conversion between two compact states. Since the microscopy technique requires dye staining, LD data for a YOYO–DNA complex obtained under similar conditions[32] were used in the comparison. The choice of the relevant period time to use from the microscopy data is not trivial. Being an ensemble average, the LD signal is expected to be a superposition of responses from molecules with a wide distribution of period times (Figure 5a). Because the distribution is asymmetric, a majority of the molecules have a cycle duration that is shorter than the average period time, but this is counteracted by the fact that fewer molecules in the tail of the distribution probably contribute with a comparatively strong LD response since they are highly stretched (Figure 8). In view of such cancelation effects we will consider it appropriate to compare the period times obtained by LD with the mean period time measured by microscopy.

B3. Effects of Field Strength, DNA Size, and Gel Concentration on the Period Time. Figure 6 shows that the time to reach the minimum orientation as measured by LD is in good agreement with the average period time obtained by microscopy, the former being about 5% longer at all field strengths. A possible cause for this small discrepancy is the difference in starting conformation in the two experiments. In the microscope the cycle time is based on the compact states formed by migration, whereas the LD times are derived from experiments on molecules that start from their equilibrium coils. For only partly equilibrated molecules, presumably more similar to migrative coils, the LD period times are 5–10% shorter.[22]

The good agreement between time to undershoot and period time in terms of both amplitude and field dependence is seen in general also with respect to the influence of gel concentration and DNA size. Table 1 shows that the period time increases with increasing DNA contour length, and the magnitudes for T7 and T2 agree fairly well with the linear relation between the LD response time and the DNA size observed by Holzwarth et al.[7] However, the value for G-phage DNA falls well below the value of ~25 s expected from a linear dependence on size, a value indeed observed by LD by Moore et al.[53] for native G-DNA. The magnitude of the period time of G-DNA thus agrees less well with LD data. This is probably related to the fact that whereas T2 DNA only occasionally forms Y-shaped conformations, the G-DNA forms Y's and a higher order of branched structures frequently, although the motion is still clearly cyclic. This behavior is more accentuated in even longer molecules,[54] and from inspection of the complex structures formed[55] it is clear that the relation between helix orientation and cycle phase is not as straight forward as for a simple U formation. Table 1 also shows that the period time increases with increasing agarose concentration in a way that is similar to the effect of gel concentration on the LD responses.[22] We conclude that, in spite of being measured from a slightly different coil state, the time to LD undershoot can be used to estimate the magnitude of the period time of the cyclic motion of DNA up to at least 164 kbp and to investigate semiquantitatively the effects of changes in gel and DNA properties on the cycle frequency.

B4. Other Studies. Masubuchi et al.[39,56] have also used fluorescence microscopy to study the periodic behavior in constant-field gel electrophoresis using ethidium bromide stained T4 DNA molecules (164 kbp). From the autocorrelation function for the radius of gyration they obtain a period time which also decreases with increasing electric field strength, but at a given field strength their values are a factor of 3–4 shorter than the average period times reported here. In their data, the time between two subsequent minima in a plot of the radius of gyration versus time gives approximately the same period time as their autocorrelation function approach, so it seems unlikely that the discrepancy between the two studies is caused by the different data evaluation procedures. The images of ethidium bromide stained T4 DNA migrating in 1% agarose presented by Howard and Holzwarth,[28] gives a typical period time of 10 s (between compact states) at 5 V/cm. This is in good agreement with our average period time (Figure 6), and again considerably longer than the 3 s observed by Masubuchi et al.[56] Since our period times are too long, we rule out the possibility that our DNA was degraded: this is also supported by the agreement with the period times derived from LD, which were measured on the major component of the T2 sample. Intercalating fluorescent dyes have been used in both studies, and at similar binding ratios, so helix extension should be approximately the same. Furthermore, both ethidium bromide (at a phosphate–dye ratio P/D = 5)[57] and YOYO (P/D = 10)[32] reduce the electrophoretic mobility of long DNA by approximately 15%, which indicates that the charge effects of the two dyes are similar. We thus have no satisfactory explanation for the discrepancy between the two studies, which however agree on the effect of gel concentration and on the fact that the buildup of U conformations is slow compared to the slipping and retraction phases of the cycle.

C. Molecular Alignment. C1. Information about the Local DNA Conformation. There are at least three independent pieces of information regarding the local DNA conformation. Firstly, as noted by several authors,[20,21,28,36] the degree of DNA stretching at various

points along the μpath can sometimes be inferred from the brightness of the molecule image. For example, since the leading parts are bright in *both* arms during U formation, and in the winning arm as the U slips and the I contracts (Figure 2), all new μpath segments are created by a head containing a DNA chain, which is in a comparatively relaxed state.

Secondly, and more quantitatively, the length of the μpath reflects how stretched the DNA is locally. L_μ for locally relaxed molecules is estimated to be approximately 7 μm (Appendix) and thus considerably shorter than typical values during migration (Figure 7a). This implies a significant stretching of the DNA polymer along the μpath, which we will quantify by comparing L_μ with the DNA contour length (see section C6 below).

Thirdly, information about the helix alignment with respect to the μpath, i.e., the degree of DNA orientation at the local level, can be obtained from LD measurements of the total helix orientation with respect to the field, provided that a correction is made for the contribution due to the global (μpath) alignment. The global orientation parameters can be estimated from the images, as will be discussed now.

C2. Separation into Global and Local LD Contributions. The main idea behind using eq 2 is that if S_{global} can be determined from the microscopy images, then a value for S_{local} can be obtained from the LD-derived value of S upon division by S_{global}. The formation of V-shaped global conformations will reduce S below 1, as seen with an S_{apex} less than unity in eq 3. However, under the present circumstances the lack of perfect orientation of the arms with respect to the field direction is a small effect and will be neglected by approximating S_{apex} in eq 3 as unity. Then S_μ alone quantifies the global orientation, so that in eq 2 $S_{global} = S_\mu$.

The factorization in eq 2 requires the orientation of the μpath segments to have cylindrical symmetry around the field,[31] which follows from the symmetry of the field. Also, the distribution of the DNA helix around the μpath segment axis has to be cylindrical, which is not necessarily true if the segment is at a non-zero angle to the field direction. We have accepted this approximation since Figure 9a shows that the μpath segments are well aligned, except possibly in the compressed states where there is little contribution to LD anyway, because S_μ is expected to be small.

The brackets in eqs 4b and 4c refer to averages along the DNA chain in the actual conformation. The averaging can be done for each orientation factor separately (as indicated in eqs 4b and 4c) if the global and local orientation distributions are independent. Since all new segments of the μpath are laid down by a relaxed (bright) head, the path is first filled with DNA with a low degree of local orientation. Only later is the DNA stretched along the μpath, as the U is pulled tight and slips into an I. The degree of local helix orientation (with respect to the μpath-segment axis) can therefore be expected to be strongly influenced by how tight the molecule is pulled along the already laid-out path but weakly correlated to how field-aligned that μpath segment is.

C3. Global Orientation. We will apply eq 3 (with $S_{apex} = 1$) to evaluate S_{local} from the S values corresponding to maximum (S_{max}) and steady state (S_{ss}) orientation determined by LD measurements (Figure 3). We therefore need to evaluate the corresponding values for S_μ.

The steady state orientation (S_{ss}) corresponds to a cycle average, so the pertinent global orientation factor is S_μ averaged over the cycle, $\langle S_\mu \rangle_{cycle}$. It is less straightforward to establish the S_μ corresponding to S_{max} (Figure 3), since it is not self-evident in which phase of the cycle there is an optimal combination of local and global alignment, giving rise to the maximum value of total helix orientation, S. However, Figure 9c shows that within experimental uncertainty there is no trend in $\cos^2 \psi'$ over the length of the arms, and furthermore, h_μ/L_μ remains approximately constant throughout the I contraction (Figure 8). These observations indicate that the segment orientation distribution is not drastically different in different parts of the μpath. This is expected since the head being in a more or less relaxed conformation whenever new segments of the μpath are laid down indicates that this is done essentially by one and the same mechanism. Thus, all extended parts of the μpath have approximately the same value of S_μ, and S_{max} therefore corresponds to the maximum value of S_{local}.

S_μ for extended conformations may be evaluated using eq 4b if the angle between the field direction and the observed μpath axis is measured segment by segment, as in Figure 9. Instead of determining the full angular distribution for all segments, we will here make use of the fact that the segment orientation for the μpath is essentially the same in all parts of the extended conformations (the situation may be different in the compact states, as discussed below). An average of $\cos \psi'$ over an I conformation can be obtained by using the observation that the ratio h_μ/L_μ is equal to $\langle \cos \psi' \rangle$, and the same argument can be applied to each of the two arms of a U conformation. We obtain $\langle \cos \psi' \rangle = 0.94 \pm 0.04$ (mean $\pm$ standard deviation (sd)) as an averge over all such extended parts of the μpath in the 60 conformations (see, e.g., h_μ/L_μ for I conformations in Figure 8). According to eq 4b it is rather $\langle \cos^2 \psi' \rangle$ which is required for calculation of S_μ, but since the distribution of ψ is narrow (Figure 9a) the equality $\langle \cos \psi' \rangle^2 = \langle \cos^2 \psi' \rangle = 0.89$ should hold to a good approximation. This was tested for five arms in three conformations, by calculating the actual value of $\langle \cos^2 \psi' \rangle$ from the full segmental orientation distribution (Figure 9b), and compared with the approximate value calculated as $\langle \cos \psi' \rangle^2 = \langle h_\mu/L_\mu \rangle^2$ for the same conformations (Table 3). At 3 V/cm the error in the assumption $\langle \cos^2 \psi' \rangle = \langle h_\mu/L_\mu \rangle^2$ is less than 5%, and since the orientation distribution should only become even narrower at higher fields, the error will be smaller, if anything, at 8 V/cm. The value of 0.89 for $\langle \cos^2 \psi' \rangle$ gives an orientation factor of $S_\mu = 0.70$ for the extended conformations, according to eq 4b.

To calculate $\langle S_\mu \rangle_{cycle}$, we need (i) the orientation factor for the extended conformations, (ii) the distribution between extended and compact conformations, and (iii) the orientation factor for the compact conformations. The compact conformations cannot be isotropic, since complete equilibration takes a much longer time (30 min)[22] than a typical cycle duration. The value $S_\mu = 0$ can therefore be used as a lower limit for the compact states, since no orientation forces perpendicular to the field direction exist. By defining unresolved conformations as all states with h_μ and $L_\mu < 15$ μm, five conformations of sixty belonged to this group, which gives a lower limit for the cycle average $\langle S_\mu \rangle_{cycle} = (5/60)0 + (55/60)0.70 = 0.64$. Table 4 summarizes the estimated orientation parameters.

Table 4. Orientation Factors from Microscopy and LD[a]

	microscopy[b]				LD[c]
	S_μ		S_{local}		S
	exp	theory[d]	exp[e]	theory[f]	exp
max	0.70 ± 0.1[g]		0.27 ± 0.03[h]		0.19
cycle av	0.64−0.70[i]	0.32	0.21−0.23[i]	0.078	0.15

[a] YOYO-stained T2 DNA (phosphate−dye ratio 10) at 8 V/cm in 1% agarose. [b] This work. [c] From eq 1, using LD[r] data from Carlsson[35]. [d] From eq 7. [e] Calculated as S/S_μ according to (3), assuming $S_{apex} = 1$ (see text). [f] From eq 14. [g] Mean ± sd is calculated by averaging eq 4b over all extended conformations, using $\langle\cos^2\psi'\rangle = \langle h/L\rangle^2$ for each arm (see text). The average of $\langle h/L\rangle$ over the arms in all extended conformations is 0.94 ± 0.04. [h] Uncertainty based on sd in S_μ. [i] Range corresponds to upper and lower estimates of S_μ for compact states (see text).

C4. Kuhn−Grün Model for Estimating Global Orientation from Microscopy Images. In a preliminary exploration of the ideas developed here,[1] a value of S_μ was calculated by the Kuhn−Grün formalism:[58]

$$S_\mu = 1 - 3\left\langle \frac{h_\mu/L_\mu}{\mathcal{L}^{-1}(h_\mu/L_\mu)} \right\rangle \quad (6)$$

where $\mathcal{L}^{-1}$ is the inverse Langevin function. It was applied[1] to a limited set of data on μpath lengths of I conformations from published microscopy images. However, because of the high fraction of U conformations created by the electrophoretic migration, this approach cannot be applied to the present more extensive data set over the whole cycle. Figure 9a shows that for a value of $h_\mu/L_\mu = 0.3$ the segment orientation distribution predicted by the freely-jointed chain, used in the Kuhn−Grün model, is considerably less biased in the field direction compared to the experimental orientation distribution of the μpath segments during electrophoresis (at a comparable value of 0.4 for h_μ/L_μ). If applied to the experimental distribution of h_μ/L_μ, the Kuhn−Grün model will therefore underestimate the tube orientation because the abundant U conformations have a high degree of μpath alignment, even for low values of the ratio h_μ/L_μ. In the present approach this problem is avoided by a model-independent evaluation of S_μ from images representing the full cycle.

C5. Tube-Orientation According to Biased Reptation Theory. Since the μpath is expected to be a reasonable approximation of the reptation tube (*vide supra*), it is interesting to compare the experimental values for S_μ with the orientation factor for the tube, S_μ^{rept}, as predicted by biased reptation theory.[59,60] The tube is laid down by the leading segment, the head, and the average tube orientation is thus equal to the average orientation of the head. The charged head segment, at an angle δ (in three dimensions) to the field, is biased by the electric forces to be preferentially in the field direction. The orientation factor can be obtained as

$$S_\mu^{rept} = \frac{3\langle\cos^2\delta\rangle - 1}{2} \quad (7)$$

where the required $\langle\cos^2\delta\rangle$ is given by[59]

$$\langle\cos^2\delta\rangle = 1 - \frac{2}{E'}\coth(E') + \frac{2}{E'^2} \quad (8)$$

The reduced electric field E′ is equal to

$$E' = Eqa/2kT \quad (9)$$

where the electric field strength E is 8 V/cm, the absolute temperature T is 300 K, k is the Boltzmann constant, and the segment length, a, is taken to be the average pore diameter (2000 Å).[51] The charge of the leading segment, q, can be estimated to be 945 electron charges from the length of YOYO-stained DNA per pore (being equal to 4500 Å as a cycle average, see L_{blob} in section C6 below) and by assuming one charge per base pair.[61] In (7)−(9) these values give $S_\mu^{rept} = 0.32$.

We also calculate the length of the tube in the field direction, $\langle L_{tube,x}\rangle$ as[59]

$$\langle L_{tube,x}\rangle = Na\langle\cos\delta\rangle = Na\left(\coth(E') - \frac{1}{E'}\right) \quad (10)$$

where the number of tube segments, N, is obtained as the DNA contour length divided by the average length of DNA per pore (4500 Å). With E' calculated as above, we obtain $\langle L_{tube,x}\rangle = 23.0$ μm, which is in fair agreement with the observed tube length (30 μm).

Our data on S_μ support the general reptation concept[2] that the μpath conformation is determined by the head via the same mechanism throughout the migration, since the segment orientation is essentially the same in all extended conformations. However, the predicted average degree of tube orientation is lower than the observed values by a factor of about 2, although it should be remembered that some tube details may be lost in the μpath. It is also difficult to find reliable estimates for the amount of DNA in the head, and an advantage with our approach is that independent experimental data (L_{blob}) can be used to estimate this parameter.

In Zimms lakes-and-straits model[12] the direction of new tube segments is the result of competition between different DNA loops in the leading end trying out cavities in different directions, in a way that is similar to the forked conformations sometimes observed for the head.[28] Interestingly, the predicted[12] total DNA orientation factor is of the same magnitude as the experimental S from LD.[22] The global and local orientation factors are not presented separately, however, so comparison with the present data is not possible.

C6. Local Helix Orientation. The maximum and cycle-averaged S_{local} is obtained as (eq 3 with $S_{apex} = 1$)

$$S_{local,max} = S_{max}/S_{\mu max} = 0.27 \quad (11a)$$

$$\langle S_{local}\rangle_{cycle} = S_{ss}/\langle S_\mu\rangle_{cycle} = 0.21-0.23 \quad (11b)$$

(see Table 4). In the absence of direct information about the distribution of the helix orientation at the local level, we invoke a second piece of information: the amount of chain length which resides below the resolution level, as given by the ratio between the DNA and μpath contour lengths L_c/L_μ. If we divide the DNA chain into N_{blob} number of blobs (Figure 10a), the amount of DNA in each blob is

$$L_{blob} = L_c/N_{blob} \quad (12)$$

The number of blobs can be estimated as

$$N_{blob} = L_\mu/a \quad (13)$$

where a is the average pore size. Using the data in Figure 7a in (12) and (13), L_{blob} is calculated to vary between 2800 Å (observed for stretched U's) and 10 000 Å (compact states), with a cycle average of 4500 Å. These considerable fluctuations in the degree of local

helix stretching over the cycle are not clearly reflected in S_{local}, its maximum value being only 20% higher than the cycle-averaged value. This is probably because quite a small fraction of the cycle is spent in the compact states (Figure 8), which therefore have a small weight in the cycle average.

From L_{blob} a corresponding value of S_{local} can be calculated on the basis of Schellman's wormlike-chain type of model for DNA.[62] For a contour length L_{blob} of DNA spanning a cavity of diameter a, the orientation factor for the helix with respect to the end-to-end vector of the DNA (i.e., the direction from entry to exit positions in the blob; see Figure 10a) is[1,63]

$$S_{local}^{WS} = \frac{3\langle\cos^2\beta\rangle - 1}{2} = \left\langle \frac{P}{L_{blob}} \frac{a^2}{\langle h_0^2\rangle} \right\rangle \qquad (14)$$

where P is the persistence length (500 Å)[43] and $\langle h_0^2\rangle$ is the average eqilibrium end-to-end distance (using $\langle h_0^2\rangle = 2P(L_{blob} - P)$[42]). The predicted cycle-averaged orientation of the helix in the blobs is calculated by averaging (14) over the distribution of L_{blob} over the cycle. Using $a = 2000$ Å, this gives $S_{local}^{WS} = 0.078$, which is a factor of about 3 smaller than the experimental value of 0.22 (eq 11b). The experimentally observed local orientation can thus be considered to be high in the sense that the DNA helix is considerably better oriented alng the μpath than expected for a wormlike chain spanning the pores.

We also used the Kuhn–Grün[58] model in eq 6 to calculate S_{local} (as is common in theoretical calculations[12,15,64])

$$S_{local}^{KG} = 1 - 3\left\langle \frac{a/L_{blob}}{\mathcal{L}^{-1}(a/L_{blob})} \right\rangle \qquad (15)$$

which gives a similar value $S_{local}^{KG} = 0.10$, as an average over the same L_{blob} data. The Kuhn–Grün model has the advantage that it is valid also for large extensions compared to the equilibrium coil size, whereas the Wilson–Schellman model has its strength in the bending properties being directly related to the helix structure. This indicates that the two models fail in this application, not because of the way DNA stiffness is accounted for, but rather because the real segment distribution is qualitatively different compared to the models. In both models the DNA conformation is represented by the field-free equilibrium chain distribution, and the field enters the present calculations only through the contour length of DNA per blob (obtained from L_μ). The real segment distribution in the blob is likely to be also directly affected by the field, most likely in terms of direct alignment of segments within the blob, giving a higher S_{local} than predicted by the models. This could arise from loops at the pore level being pulled out by the field to point in the field direction (Figure 10b), as has been suggested from other observations.[1,46] Such loop formation would give rise to a high helix orientation for the DNA in the blob compared to its end-to-end distance, in a way that is similar to the high degree of orientation of the μpath compared to its end-to-end distance, that arises because of U formation at the global level.

C7. Tube Contributions to the Effective Friction Coefficient in Gels. The electrophoretic mobility μ is given by

$$\mu = v/E = Q/f \qquad (16)$$

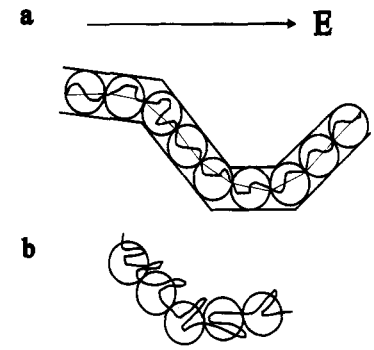

Figure 10. (a) Blob model for DNA in gels. The blob diameter is equal to the average pore diameter, a. Each blob contains L_{blob} of the contour length of DNA. (b) Local loops stretched in the field direction.

where v is the center-of-mass velocity, Q is the electrophoretic charge of DNA, and f is the friction coefficient. In solution f is the hydrodynamic friction during electrophoresis, whereas in gels f is an effective friction coefficient for macroscopic transport of the center of mass. The mobility of YOYO-stained T2 DNA in 1% agarose at 8 V/cm is[32] 6.6×10^{-5} cm^2 V^{-1} s^{-1}, and using an electrophoretic charge of 1 electron charge per base pair[61] one obtains $f = 4.0 \times 10^{-3}$ g/s. The friction coefficient in solution can similarly be calculated to be 0.79×10^{-3} g/s using a mobility of 33×10^{-5} cm^2 V^{-1} s^{-1} for native DNA at the present ionic strength.[65]

At this field strength the effective friction coefficient in the gel is higher than in solution by a factor of about 5. According to reptation theories, DNA molecules in gels migrate slower than in solution because they must follow the reptation tube, which will not provide the shortest path in the field direction, unless the tube is perfectly aligned. This detour effect is expressed by adding a geometrical factor to eq 16[2]

$$\mu = \frac{Q}{\xi}\left\langle \frac{h_x^2}{L_{tube}^2} \right\rangle \qquad (17)$$

where L_{tube} and h_x are the contour length and field projection of the end-to-end vector of the tube, respectively, and ξ is the friction coefficient for motion along the tube. Simulations indicate that (17) applies even if there are strong fluctuations in the tube length,[2] which is the case, as observed experimentally (Table 2). Assuming, that the μpath reflects the reptation tube, the experimental mobilities can be corrected for the detour effect and thus the tube friction coefficient ξ can be estimated. Using the value 0.25 for $\langle h_\mu^2/L_\mu^2\rangle$ averaged over the cycle (Table 2) gives a friction coefficient $\xi = 0.99 \times 10^{-3}$ g/s, which is close to the value in free solution. This rather crude approach thus suggests that the friction for motion in the tube is about the same as the hydrodynamic friction in solution. This finding is consistent with the observation that the temperature dependence in the electrophoretic mobility is very similar to that of water viscosity.[66]

Conclusions

The migration of DNA molecules between 38 and 740 kbp through agarose gels is periodic. The distribution of period times is wide, with a standard deviation equal to half the average, and asymmetric with a long-time tail.

The average period time decreases with increasing field strength and increases with increasing gel concentration and DNA contour length. The period times measured by microscopy and linear dichroism agree well for DNA of 38 and 164 kbp, but not for 740 kbp, which shows that for intermediately sized DNA LD can be used to evaluate the period time.

Averaged over the cycle, the apparent DNA length L_μ (30 μm for T2 DNA at 8 V/cm) is 40% of the DNA contour length, which shows that a large fraction of the DNA chain conformation ("the local conformation") resides below the resolution of the microscope and has to be studied by other methods.

The DNA path in the gel as imaged at the resolution of the microscope (the "global" path) is strongly aligned with the field (cycle-averaged global orientation factor 0.67 ± 0.03 at 8 V/cm). The degree of orientation is essentially the same in all elongated conformations, in accordance with reptation theory, but the cycle-averaged orientation factor is about 2 times higher than predicted by biased reptation models. Resolution limitations prevent a definitive comparison with reptation theories, however.

Over the major part of the cycle L_μ is several times longer than for a locally relaxed chain, which indicates that there is a considerable degree of local stretching of the DNA chain along the path in the gel, in agreement with spectroscopic studies of helix alignment.[64] The stretching is due to long residence time in the U conformations, and to that only a small fraction of the cycle time is spent in conformations which are compatible with a locally relaxed chain.

The local orientation factor for the helix with respect to the global path is 0.22 ± 0.01, or a factor of about 3 higher than expected for a wormlike chain spanning an average pore. This indicates that, in addition to the stretching of the chain locally due to U formation, there is direct field alignment of helix loops at the pore level.

The estimated friction coefficient for motion along the reptation tube is close to the value observed for electrophoresis in solution.

Acknowledgment. Financial support from the Hasselblad and Magn. Bergwall foundations and the Swedish Technical Research council is gratefully acknowledged. We are thankful to Dr. Mats Jonsson, Dr. Carl-Fredrik Burman, Dr. Eimer Tuite, and the referees for helpful suggestion and M. Sc. Christina Carlsson for providing experimental LD data before publication and for helpful discussions.

Appendix. Projection Effects

Length and End-to-End Distance of the μpath. Due to the molecule image being a projection of the three-dimensional molecular path onto the image plane, the measured values of L_μ and h_μ will be lower than the true values. The orientation distribution of the μpath segments (Figure 9a) is quite narrow in the plane of focus, however, and by symmetry the distribution is the same in any plane that contains the field direction.[31] The average of cos ψ' over the distribution is equal to 0.94 (Table 4), so the projection underestimates the values of properties that stretch over many μpath segments, such as L_μ and h_μ, by approximately 5–10%. Projection effects can therefore be considered to be small in extended conformations.

In compact conformations there is the additional effect that the μpath cannot be traced when it folds over itself in the projected images. The apparent L_μ below which such overlap effects become serious can be estimated from the fact that compact states are formed by a distinct process, which is similar to a field-free relaxation. Other studies[22,36,64] indicate that the complete field-free relaxation consists of a fast DNA retraction along the original path over seconds. This results in a locally relaxed, but still elongated and field-aligned, DNA coil, which only over minutes to hours becomes isotropic. The second step of the field-free relaxation is slow compared to the cycle time scale, so that during migration the locally relaxed coil (resulting from the I retraction) changes shape not by slow Brownian tube motion but by the field starting to pull out a new U to create a new tube. It is during this rearrangement of the locally relaxed chain that overlap effects are severe, and their onset can be anticipated to occur when the μpath length is approaching the length of a locally relaxed chain. Gurrieri et al.[36] have measured the μpath length of T2 DNA to be 6.9 ± 1.8 μm after 2–10 s of field-free relaxation which, in view of the spectroscopically determined relaxation time scales,[64] can be expected to be a good approximation of the μpath length corresponding to a locally relaxed T2 DNA chain under the present conditions. Overlap effects become small again when the arms of the new U emerges, i.e. when h_μ is larger than the typical compact coil size. For the purposes of this study we conclude that when the apparent L_μ and h_μ values are smaller than 10 μm, the true values are probably higher, and the actual conformation of the μpath is unknown.

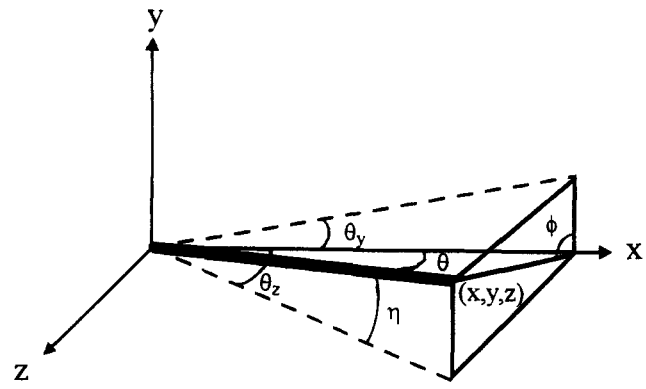

Figure 11. Definition of conventional polar angles ϕ and θ, for describing the orientation of a helix segment (thick line), and of angles θ_z, θ_y, and η used in the analysis of projection effects in LD. The field direction is along the x-axis, and the light in LD and microscopy propagates along the y-axis, with the microscopy image in the xz-plane.

Projection Effects in LD. The orientation factor S in eq 1 quantifies the orientation of the helix axis with respect to the field direction and is related to the angle θ between the three-dimensional path of the DNA helix and the direction of the field through the relation[31]

$$S = (3\langle\cos^2\theta\rangle - 1)/2 \qquad \text{(A1)}$$

In this appendix eq A1 is converted into the expression (A7) containing the angle θ_z between the field direction and the *projection* of the helix axis onto the plane of focus, which is the angle that can be measured with microscopy. It is therefore necessary to express $\langle\cos^2\theta\rangle$ in terms of $\langle\cos^2\theta_z\rangle$.

Instead of using the conventional polar angles θ and ϕ (see Figure 11) the orientation of a segment of DNA can be expressed in terms of the angles θ_z and θ_y between the electric field direction x and the projection

of the segment onto the xz (plane of focus) and xy planes, respectively (the light enters along the y direction in both LD and microscopy). The advantage of this representation is that, due to the axial symmetry of the field, the distribution of θ_y is the same as for θ_z (about which information can be obtained by microscopy) and, thus

$$\langle \cos^2 \theta_y \rangle = \langle \cos^2 \theta_z \rangle \tag{A2}$$

Let a segment of unit length have one end at (x, y, z). With η being the angle between the segment and the xz plane, identification of x as expressed in the two angle sets gives

$$\cos^2 \theta = x^2 = \cos^2 \eta \cos^2 \theta_z \tag{A3}$$

It is required that $\cos^2 \eta$ be expressed in θ_y and θ_z, which can be obtained by identifying y/x as expressed in the two sets of angles:

$$\tan \theta_y = \frac{y}{x} = \frac{\sin \eta}{\cos \eta \cos \theta_z}$$

or

$$\cos^2 \eta = \frac{1}{1 + \tan^2 \theta_y \cos^2 \theta_z} \tag{A4}$$

(A3) and (A4) give

$$\cos^2 \theta = \frac{\cos^2 \theta_z \cos^2 \theta_y}{\cos^2 \theta_y + \cos^2 \theta_z (1 - \cos^2 \theta_y)} \tag{A5}$$

For the average over an ensemble of such segments we can use (A2) in (A5) which gives the desired relation:

$$\langle \cos^2 \theta \rangle = \frac{\langle \cos^2 \theta_z \rangle}{2 - \langle \cos^2 \theta_z \rangle} \tag{A6}$$

The orientation factor S in (A1) is then given by

$$S = \frac{3\langle \cos^2 \theta \rangle - 1}{2} = \frac{2\langle \cos^2 \theta_z \rangle - 1}{2 - \langle \cos^2 \theta_z \rangle} \tag{A7}$$

This derivation applies to the second moment of a cylindrically symmetric distribution of any type of segment. In this study, eq A7 is used in obtaining eq 4b for the orientation factor of the μpath, by setting θ equal to ψ (and $\theta_z = \psi'$), the angle between the μpath segments and the field. The denominator in (A6) shows that the correction due to projection effects is usually quite small since a typical value for $\langle \cos^2 \psi' \rangle$ for electrophoretic orientation is 0.8 (Table 3).

Equation A7 is also used to obtain eq 4a for the orientation factor S_{apex} corresponding to the angle γ' between each arm of a V conformation and the field. By field symmetry, V conformations will form in a cylindrically symmetric fashion around the field direction, and projection effects have to be corrected by applying (A7) with $\theta = \gamma$, and $\theta_z = \gamma'$ as measured in the image plane.

References and Notes

(1) Norden, B.; Elvingson, C.; Jonsson, M.; Åkerman, B. *Q. Rev. Biophys.* **1991**, *24*, 103–164.
(2) Zimm, B. H.; Levene, S. D. *Q. Rev. Biophys.* **1992**, *25*, 171–204.
(3) Viovy, J. L. *Contemp. Phys.* **1992**, *33*, 25–40.
(4) Schwartz, D. C.; Saffran, W.; Welch, J.; Haas, M.; Goldenberg, M.; Cantor, C. R. *Cold Spring Harbon Symp. Quant. Biol.* **1983**, *47*, 189–195.
(5) Carle, G. F.; Frank, M.; Olson, M. V. *Science* **1986**, *232*, 65–68.
(6) Åkerman, B.; Jonsson, M.; Nordén, B. *J. Chem. Soc., Chem. Commun.* **1985**, 422–423.
(7) Holzwarth, G.; McKee, C. B.; Steiger, S.; Crater, G. *Nucl. Acids Res.* **1987**, *15*, 10031–10045.
(8) Platt, K.-J.; Holzwarth, G. *Phys. Rev. A* **1989**, *40*, 7292–7300.
(9) Crater, G. D.; Gregg, M. R.; Holwarth, G. *Electrophoresis* **1989**, *10*, 310–315.
(10) Åkerman, B.; Jonsson, M. *J. Phys. Chem.* **1990**, *94*, 3228–3838.
(11) Whitcomb, R. W.; Holzwarth, G. *Nucl. Acids Res.* **1990**, *18*, 6331–6338.
(12) Zimm, B. H. *J. Chem. Phys.* **1991**, *94*, 2187–2206; **1991**, *95*, 3026.
(13) Deutsch, J. M. *Science* **1988**, *240*, 922–924.
(14) Duke, T. A. *Phys. Rev. Lett.* **1989**, *62*, 2877–2880.
(15) Smith, S. B.; Heller, C.; Bustamante, C. *Biochemistry* **1991**, *30*, 5264–5274.
(16) Madden, T. L.; Deutsch, J. M. *J. Chem. Phys.* **1991**, *94*, 1584–1591.
(17) Kotaka, T.; Adachi, S.; Shikata, T. *Electrophoresis* **1993**, *14*, 313–321.
(18) Deutsch, J. M. *J. Chem. Phys.* **1989**, *90*, 7436–7441.
(19) Zimm, B. H. *Phys. Rev. Lett.* **1988**, *61*, 2965–2968.
(20) Smith, S. B.; Aldridge, P. K.; Callis, J. B. *Science* **1989**, *243*, 203–206.
(21) Schwartz, D. C.; Koval, M. *Nature* **1989**, *338*, 520–522.
(22) Åkerman, B.; Jonsson, M.; Nordén, B.; Lalande, M. *Biopolymers* **1989**, *28*, 1541–1571.
(23) Åkerman, B.; Jonsson, M.; Moore, D.; Schellman, J. C. *Curr. Commun. Cell Mol. Biol.* **1990**, *1*, 23–41.
(24) Magnúsdóttir, S.; Åkerman, B.; Jonsson, M. *J. Phys. Chem.* **1994**, *98*, 2624–2633.
(25) Bustamante, C. *Annu. Rev. Biophys. Biophys. Chem.* **1991**, *20*, 415–446.
(26) Houseal, T. W.; Bustamante, C.; Stump, R. F.; Maestre, M. F. *Biophys. J.* **1989**, *56*, 507–516.
(27) Keiner, L. E.; Holzwarth, G. *J. Chem. Phys.* **1992**, *97*, 4476–4484.
(28) Howard, T. D.; Holzwarth, B. *Biophys. J.* **1992**, *63*, 1487–1492.
(29) Donelli, G.; Dore, E.; Frontali, C.; Brandolf, M. E. *J. Mol. Biol.* **1975**, *94*, 555–565.
(30) Smith, S. B.; Gurrieri, S.; Bustamante, C. *Curr. Commun. Cell Mol. Biol.* **1990**, *1*, 55–79.
(31) Nordén, B. *Appl. Spectrosc. Rev.* **1978**, *14*, 157–248.
(32) Carlsson, C.; Larsson, A.; Jonsson, M. Manuscript in preparation.
(33) Larsson, A.; Carlsson, C.; Jonsson, M.; Albinsson, B. *J. Am. Chem. Soc.* **1994**, *116*, 8459–8465.
(34) Carlsson, C.; Larsson, A.; Jonsson, M.; Albinsson, B.; Nordén, B. *J. Phys. Chem.* **1994**, *98*, 10313–10321.
(35) Carlsson, C. Personal communication.
(36) Gurrieri, S.; Rizzarelli, E.; Beach, D.; Bustamante, C. *Biochemistry* **1990**, *29*, 3396–3401.
(37) Rampino, N. J.; Chrambach, A. *Biopolymers* **1991**, *31*, 1297–1307.
(38) Rampino, N. J. *Biopolymers* **1991**, *31*, 1009–1016.
(39) Masubuchi, Y.; Oana, H.; Ono, K.; Matsumoto, M.; Doi, M.; Minagawa, K.; Matsuzawa, K.; Yoshikawa, K. *Macromolecules* **1993**, *26*, 5269–5270.
(40) Snedecor, G. W.; Cochran, W. G. *Statistical Methods*; Iowa State University Press: Ames, IA, 1989.
(41) Butour, J. L.; Delain, E.; Couland, D.; LePeqc, J.-B.; Barbet, J.; Roques, B. P. *Biopolymers* **1978**, *17*, 873–886.
(42) Bloomfield, V. A.; Crother, D. M.; Tinoco, I. *Physical Chemistry of Nucleic Acids*; Harper & Row: New York, 1974.
(43) Hagerman, P. J. *Annu. Rev. Biophys. Biophys. Chem.* **1988**, *17*, 265–286.
(44) Stellwagen, N. C. *J. Biomol. Struct. Dyn.* **1985**, *3*, 299–314.

(45) Parus, S. J.; Shick, R. A.; Matsumura, M.; Morris, M. D. *Anal. Chem.* **1988**, *60*, 1635–1637.
(46) Turmel, C.; Brassard, E.; Slater, G. W.; Noolandi, J. *Nucl. Acids Res.* **1990**, *18*, 569–575.
(47) Yanagida, M.; Morikawa, K.; Hiraoka, Y.; Matsumoto, S.; Uemura, T.; Okada, S. In *Applications of Fluorescence in the Biomedical Sciences*; Liss, A. R., Ed.; Wiley-Liss: New York, **1986**; pp 321–345.
(48) Matsumoto, M.; Sakaguchi, T.; Kimura, H.; Doi, M.; Minagawa, K.; Matsuzawa, K.; Yoshikawa, K. *J. Polym. Sci. B, Polym. Phys.* **1992**, *30*, 779–783.
(49) Carlsson, C.; Larsson, A.; Jonsson, M.; Nordén, B. *J. Am. Chem. Soc.* **1995**, *117*, 3871–3872.
(50) Perkins, T. T.; Smith, D. E.; Chu, S. *Science* **1994**, *264*, 819–822.
(51) Serwer, P. *Electrophoresis* **1983**, *4*, 375–382.
(52) Song, L.; Maestre, M. F. *J. Biomol. Struct. Dyn.* **1991**, *9*, 87–99.
(53) Moore, D. P. B.A. Thesis, University of Oregon, Eugene, OR, 1986.
(54) Bustamante, C.; Gurrieri, S.; Smith, S. B. *Trends Biotechnol.* **1993**, *11*, 23–30.
(55) Duke, T. A. J.; Viovy, J. L. *Phys. Rev. Lett.* **1992**, *68*, 542–547.
(56) Oana, H.; Masubuchi, Y.; Matsumoto, M.; Doi, M.; Matsuzawa, Y.; Yoshikawa, K. *Macromolecules* **1994**, *27*, 6061–6067.
(57) Reese, H. R. *Biopolymers* **1994**, *34*, 1349–1358.
(58) Kuhn, W.; Grün, F. *Kolloid Z.* **1942**, *101*, 248–271.
(59) Lumpkin, O. J.; Déjardin, P.; Zimm, B. H. *Biopolymers* **1985**, *24*, 1573–1593.
(60) Slater, G. W.; Noolandi, J. *Biopolymers* **1986**, *25*, 431–454.
(61) Schellman, J. A.; Stigter, D. *Biopolymers* **1977**, *16*, 1415–1434.
(62) Schellman, J. A. *Biopolymers* **1974**, *13*, 217–226.
(63) Wilson, R. W.; Schellman, J. A. *Biopolymers* **1977**, *16*, 2143–2165.
(64) Mayer, P.; Sturm, J.; Weill, G. *Biopolymers* **1993**, *33*, 1347–1357.
(65) Hartford, S. L.; Flygare, W. H. *Macromolecules* **1975**, *8*, 80–83.
(66) Hervet, H.; Bean, C. P. *Biopolymers* **1987**, *26*, 727–742.

MA946249G